View metadata, citation and similar papers at core.ac.uk

brought to you by CORE

provided by Publications Server of the Weierstrass Institute for Applied Analysis and Stochastics

Weierstraß-Institut
für Angewandte Analysis und Stochastik

im Forschungsverbund Berlin e.V.

Preprint ISSN 0946 – 8633

Simulation of microwave circuits and laser structures including PML by means of FIT

Georg Hebermehl[1], Jürgen Schefter[2], Rainer Schlundt[2],

Thorsten Tischler[3], Horst Zscheile[3], Wolfgang Heinrich[3]

submitted: 5th February 2004

[1] Greifswalder Str. 147
10409 Berlin
Germany

[2] Weierstrass-Institute for Applied
Analysis and Stochastics
Mohrenstraße 39
10117 Berlin, Germany
E-Mail: schefter@wias-berlin.de
schlundt@wias-berlin.de

[3] Ferdinand-Braun-Institut für Höchstfrequenztechnik
Albert-Einstein-Str. 11, 12489 Berlin, Germany
E-Mail: tischler@fbh-berlin.de
zscheile@fbh-berlin.de
w.heinrich@ieee.org

No. 905
Berlin 2004

2000 *Mathematics Subject Classification.* 35Q60, 65N22, 65F15, 65F10.

Key words and phrases. Microwave device, Semiconductor laser, Simulation, Maxwell's equations, Boundary value problem, PML boundary condition, Eigenvalue problem, Linear algebraic equations, Rectangular grids, Tetrahedral nets.

Edited by
Weierstraß-Institut für Angewandte Analysis und Stochastik (WIAS)
Mohrenstraße 39
10117 Berlin
Germany

Fax: + 49 30 2044975
E-Mail: preprint@wias-berlin.de
World Wide Web: http://www.wias-berlin.de/

Abstract

Field-oriented methods which describe the physical properties of microwave circuits and optical structures are an indispensable tool to avoid costly and time-consuming redesign cycles. Commonly the electromagnetic characteristics of the structures are described by the scattering matrix which is extracted from the orthogonal decomposition of the electric field. The electric field is the solution of an eigenvalue and a boundary value problem for Maxwell's equations in the frequency domain. We discretize the equations with orthogonal grids using the Finite Integration Technique (FIT). Maxwellian grid equations are formulated for staggered nonequidistant rectangular grids and for tetrahedral nets with corresponding dual Voronoi cells. The interesting modes of smallest attenuation are found solving a sequence of eigenvalue problems of modified matrices. To reduce the execution time for high-dimensional problems a coarse and a fine grid is used. The calculations are carried out, using two levels of parallelization. The discretized boundary value problem, a large-scale system of linear algebraic equations with different right-hand sides, is solved by a block Krylov subspace method with various preconditioning techniques. Special attention is paid to the Perfectly Matched Layer boundary condition (PML) which causes non physical modes and a significantly increased number of iterations in the iterative methods.

Contents

List of Figures

1 Introduction

The commercial applications of microwave circuits cover the frequency range between 1 GHz and about 100 GHz; special applications, e.g. in radioastronomy, use even higher frequencies up to 1 THz. For optoelectronic devices, frequencies around several hundred THz are common. Higher frequencies lead to decreasing wavelength. Thus they yield increased dimensions of the discretization corresponding to the numerical problem and demand new strategies.

The subject under investigation are three-dimensional structures of arbitrary geometry which are connected to the remaining circuit by transmission lines. Ports are defined at the transmission-lines outer terminations. In order to characterize their electrical behavior the transmission lines are assumed to be infinitely long and longitudinally homogeneous. Short parts of the transmission lines and the passive structure (discontinuity) form the structure under investigation. The entire structure has to be covered with an enclosure.

2 Scattering matrix

The scattering matrix describes the structure in terms of wave modes on the transmission line sections at the ports. The dimension of this matrix is determined by the total number of modes at all ports. The scattering matrix can be extracted from

the orthogonal decomposition of the electric field. This has to be done at a pair of neighboring planes z_p and $z_{p+\Delta p}$ on each waveguide [2, 5]. The electric fields at the cross-sectional planes z_p and $z_{p+\Delta p}$ are known from the solution of the eigenvalue problem (see section 5) and from the computation of the boundary value problem (see section 3), respectively.

3 Boundary value problem

A three-dimensional boundary value problem can be formulated using the integral form of Maxwell's equations in the frequency domain in order to compute the electromagnetic field:

$$\begin{aligned} \oint_{\partial\Omega} \vec{H} \cdot d\vec{s} &= \int_{\Omega} \jmath\omega[\epsilon]\vec{E} \cdot d\vec{\Omega}, \\ \oint_{\partial\Omega} \vec{E} \cdot d\vec{s} &= -\int_{\Omega} \jmath\omega[\mu]\vec{H} \cdot d\vec{\Omega}, \end{aligned} \tag{1}$$

$$\vec{D} = [\epsilon]\vec{E}, \quad \vec{B} = [\mu]\vec{H}, \tag{2}$$

with

$$[\epsilon] = \epsilon_0 \mathrm{diag}\left(\tilde{\epsilon}_x, \tilde{\epsilon}_y, \tilde{\epsilon}_z\right), \quad [\mu] = \mu_0 \mathrm{diag}\left(\tilde{\mu}_x, \tilde{\mu}_y, \tilde{\mu}_z\right). \tag{3}$$

for rectangular grids and

$$[\epsilon] = \epsilon_0 \epsilon_r, \quad [\mu] = \mu_0 \mu_r \tag{4}$$

for tetrahedral grids. The electric field intensity $\vec{D}$ and the magnetic flux density $\vec{B}$ are complex functions of the spatial coordinates. ω is the angular frequency of the sinusoidal excitation, and $\jmath^2 = -1$. Ω is an open surface surrounded by a closed contour $\partial\Omega$. The direction of the element $d\vec{s}$ of the contour $\partial\Omega$ is determined according to a right-hand system.

At the port p the transverse electric field $\vec{E}_t(z_p)$ is given by superposing the fields of the weighted transmission line modes $\vec{E}_{t,l}(z_p)$:

$$\vec{E}_t(z_p) = \sum_{l=1}^{m^{(p)}} w_l(z_p)\vec{E}_{t,l}(z_p). \tag{5}$$

The transverse electric mode fields $E_{t,l}(z_p)$ have to be computed solving an eigenvalue problem for the transmission lines (see section 5). All other parts of the surface of the computation domain are assumed to be electric or magnetic walls:

$$\vec{E} \times \vec{n} = 0 \quad \text{or} \quad \vec{H} \times \vec{n} = 0. \tag{6}$$

In order to simulate open structures we apply the PML absorbing boundary condition. The uniaxial formulation according to [9] is implemented. The PML provides absorbing properties for any frequency, polarization and angle of incidence. Its layers are filled with an artificial material with complex anisotropic material properties. Therefore, the complex permittivity $[\epsilon]$ and the complex permeability $[\mu]$ are diagonal tensors (see (3)). ϵ_0 and μ_0 are the permittivity and the permeability in vacuum, respectively.

4 Maxwellian grid equations

Maxwell's equations are discretized on staggered grids using the Finite Integration Technique with lowest order integration formulae

$$\oint_{\partial\Omega} \vec{f} \cdot d\vec{s} \approx \sum(\pm f_i s_i), \quad \int_{\Omega} \vec{f} \cdot d\vec{\Omega} \approx f\Omega. \tag{7}$$

In the following we refer to staggered nonequidistant rectangular grids [1, 14, 7] or tetrahedral nets with corresponding Voronoi cells [10].

4.1 Staggered nonequidistant rectangular grids

The use of rectangular grids is the standard approach. In general it is very well adapted to planar microwave structures, since most circuits have a rectangular geometry.

Using (7) for staggered nonequidistant rectangular grids Eqs. (1) are transformed into a set of grid equations:

$$\begin{aligned} A^T D_{s/\tilde{\mu}} \vec{b} &= \jmath\omega\epsilon_0\mu_0 D_{A_{\tilde{\epsilon}}} \vec{e}, \\ A D_s \vec{e} &= -\jmath\omega D_A \vec{b}. \end{aligned} \tag{8}$$

The vectors $\vec{e}$ and $\vec{b}$ contain the components of the electric field intensity and of the magnetic flux density of the elementary cells, respectively. The diagonal matrices $D_{s/\tilde{\mu}}$, $D_{A_{\tilde{\epsilon}}}$, D_s, and D_A contain the information on cell dimensions and materials. A is sparse and contains the values 0, 1, and -1 only.

Eliminating the components of the magnetic flux density from the two equations (8) the number of unknowns can be reduced by a factor of two, and we obtain the system of linear algebraic equations

$$(A^T D_{s/\tilde{\mu}} D_A^{-1} A D_s - k_0^2 D_{A_{\tilde{\epsilon}}})\vec{e} = 0, \;\; k_0 = \omega\sqrt{\epsilon_0\mu_0}\,. \tag{9}$$

Taking into account the boundary conditions, (9) can be written as

$$\tilde{A}\vec{e} = \vec{r}\,, \tag{10}$$

where the vector $\vec{r}$ contains the boundary values of the electric field according to Eqs. (5) and (6). An example is demonstrated in [6]. k_0 is the wavenumber in vacuum, which is proportional to the frequency ω.

4.2 Tetrahedral nets and Voronoi cells

Because of the high spatial resolution CPU time and storage requirements are very high. Using rectangular grids a mesh refinement in one point results in an accumulation of small elementary cells in all coordinate directions even though generally the

refinement is needed only in inner regions. In addition, rectangular grids are not well suited for treatment of curved and non-rectangular structures. Thus, an additional finite-volume method was developed, which uses tetrahedral nets with corresponding Voronoi cells for the three-dimensional boundary value problem. This allows to reduce the number of elementary cells by local grid refinement and improves the treatment of curved structures. The primary grid is formed by tetrahedra and the dual grid by the corresponding Voronoi cells (see Fig. 1).

For sake of simplicity, at first, we assume in this paper that the circumcenter of a tetrahedron is located within the tetrahedron. We consider a tetrahedron $ABCD$ with the internal edge AB (see Fig. 2) and the neighbouring elements, which share the edge AB with it (see Fig. 3).

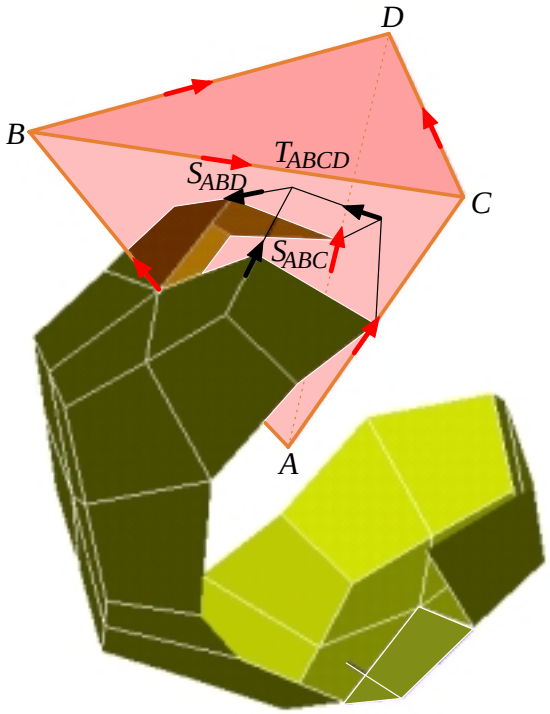

Figure 1: Voronoi cell and single tetrahedron

The electric field intensity components (marked with red color in Fig. 1 and in Fig. 2) are located at the centers of the edges of the tetrahedra, and the magnetic flux density components (marked with black color) are normal to the circumcenters of the triangular faces. The Voronoi cells are polytopes. In the special case demonstrated in Fig. 1 the Voronoi cell is a pentadodecahedron which results as dual cell from 20 neighboring regular tetrahedra.

We use the following notations (see Fig. 1, 2, and 3) with $X, Y, Z, W \in \{A, B, C, D\}$, where X, Y, Z, W are different from each other, in order to develop the grid equations for tetrahedral nets:

X, Y, Z, W	nodes,
XY	edge between the nodes X and Y,
XYZ	triangle,
$XYZW$	tetrahedron,
S_{XY}	center of XY,
S_{XYZ}	circumcenter of the triangle XYZ,
T_{XYZW}	circumcenter of the tetrahedron $XYZW$,
E_{XY}	magnitude of the electric field on S_{XY} between the nodes X and Y,
B_{XYZ}	magnitude of the magnetic flux density on S_{XYZ}, normal to XYZ,
$\mu_{XYZW} = \mu_0\mu_r$	permeability in $XYZW$,
$\epsilon_{XYZW} = \epsilon_0\epsilon_r$	permittivity in $XYZW$,
l_{XY}	distance of node X to node Y,
l^W_{XYZ}	distance of the circumcenter of $XYZW$ to the face XYZ,
d^Z_{XY}	distance of the circumcenter of XYZ to the edge XY,
a_{XYZ}	area of triangle XYZ.

E_{XY} and B_{XYZ} satisfy

$$\begin{aligned} E_{XY} &= -E_{YX}, \\ B_{XYZ} = B_{YZX} = B_{ZXY} &= -B_{YXZ} = -B_{XZY} = -B_{ZYX}, \end{aligned} \tag{11}$$

respectively.

Using a finite volume approach with the lowest-order integration formulae (7) Eqs. (1) are transformed into a set of grid equations.

Taking into account the constitutive relations (2) the first equation of (1) is discretized on the dual grid. The internal edge AB is orthogonal to the corresponding Voronoi cell face over which we have to integrate (see Fig. 1). The closed integration path $\partial\Omega$ (see (1) and (7)) consists of the edges with length $s_i = l^W_{XYZ}$ (see (7) and Fig. 2), and is the polygon around the periphery of the mentioned Voronoi cell face (see Fig. 1, upper pentagon). The vertices of the polygon are the circumcenters of the tetrahedra which share the edge AB with the tetrahedron $ABCD$ (see Fig. 3). $f_i = B_{XYZ}$ denotes the function values on S_{XYZ} (see Fig. 2). Ω is the area of the Voronoi cell face. $f = E_{AB}$ denotes the function value on the center S_{AB}. Thus, the discretized equation takes the form:

$$\begin{aligned} &\textstyle\sum_{CD} \frac{1}{\mu_{ABCD}} \left[l^D_{ABC}\, B_{ABC} + l^C_{ABD}\, B_{ABD} \right] = \\ &\jmath\omega \left[\textstyle\sum_{CD} \frac{1}{2} \epsilon_{ABCD} \left(d^C_{AB}\, l^D_{ABC} + d^D_{AB}\, l^C_{ABD} \right) \right] E_{AB} \end{aligned} \tag{12}$$

where the sum is over those tetrahedra $ABCD$, which share the edge AB (see Fig. 3).

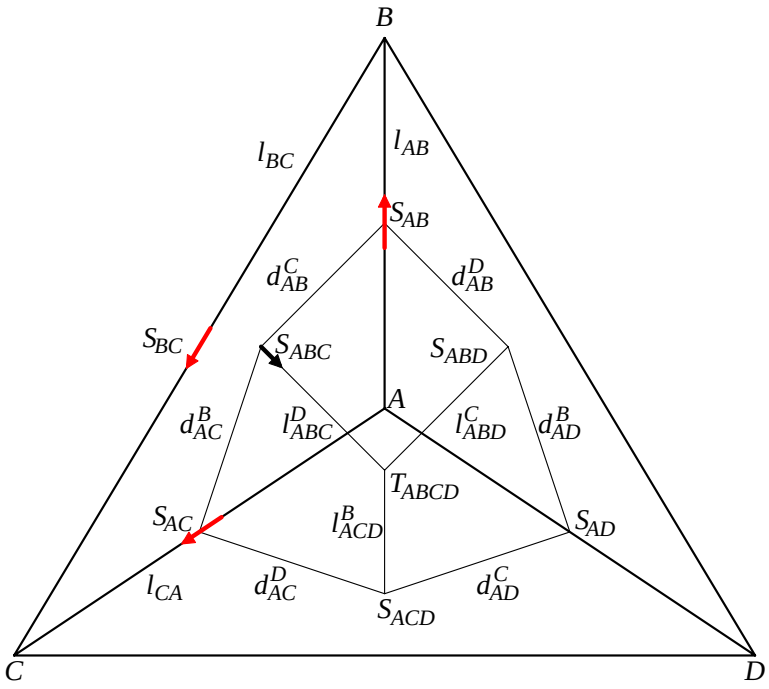

Figure 2: Tetrahedron with partial areas of the Voronoi cell faces, which correspond to node A

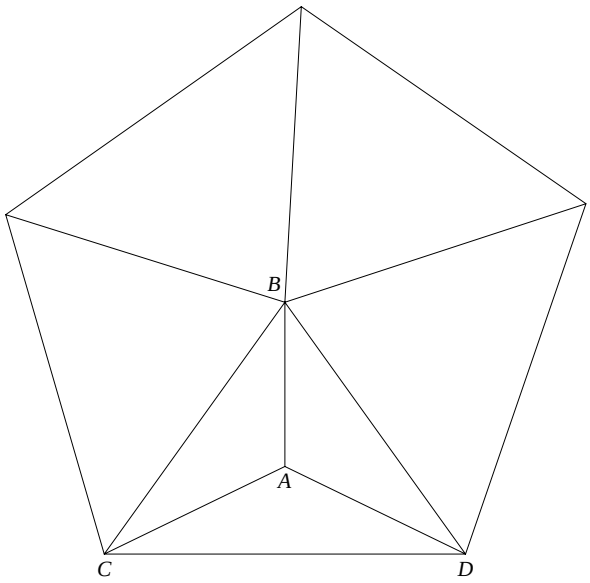

Figure 3: Tetrahedra which share the edge AB

The second equation of (1) is discretized using (7) on the primary grid. We have to integrate over the triangle ABC, i.e., the closed integration path $\partial\Omega$ consists of the edges with length $s_i = l_{XY}$ and is the polygon around the periphery of the mentioned triangle. $f_i = E_{XY}$ denotes the function value on the edges XY. Ω is the area a_{ABC} of the triangle ABC. $f = B_{ABC}$ denotes the function value on the circumcenter S_{ABC} of the triangle ABC. This yields the following form:

$$l_{AB}\, E_{AB} + l_{BC}\, E_{BC} + l_{CA}\, E_{CA} = -\jmath\omega a_{ABC}\, B_{ABC}. \tag{13}$$

Now we address the first of the surface integrals

$$\oint_{\cup\Omega} ([\epsilon]\vec{E}) \cdot d\vec{\Omega}{=}0, \quad \oint_{\cup\Omega} ([\mu]\vec{H}) \cdot d\vec{\Omega}{=}0, \tag{14}$$

reverting to the dual grid. In (14) $\cup\Omega$ is a closed surface with an interior volume. We have to integrate over the surface of the Voronoi cell. The surface of the Voronoi cell consists of all partial Voronoi areas, which belong to tetrahedron edges, whose shared corner node is A (see Fig. 1, 2 and 3). A discretization formula, with similar form to the right-hand side of (12) is obtained, i.e.,

$$\sum_B \left(\left[\sum_{CD} \frac{1}{2} \epsilon_{ABCD} \left(d^C_{AB}\, l^D_{ABC} + d^D_{AB}\, l^C_{ABD} \right) \right] E_{AB} \right) = 0, \tag{15}$$

except for the additional outer summation taken over all the nodes B neighboring A (in the primary grid).

For our final integral equation (14) the primary grid is used again, but now the integration is over the surface of the tetrahedron $ABCD$. As a consequence, the discretized form

$$-a_{ABC}\, B_{ABC} - a_{ACD}\, B_{ACD} + a_{ABD}\, B_{ABD} + a_{BCD}\, B_{BCD} \;=\; 0 \tag{16}$$

can be deduced.

Eqs. (12) and (13) form a system of linear algebraic equations for the computation of the electromagnetic field. Substituting the components of the magnetic flux density the number of unknowns in this system can be reduced by a factor of two:

$$\begin{aligned} &\textstyle\sum_{CD} \frac{1}{\mu_{ABCD}} \left[\left(\frac{l^D_{ABC}}{a_{ABC}} + \frac{l^C_{ABD}}{a_{ABD}} \right) l_{AB}\, E_{AB} + \right. \\ &+ \frac{l^D_{ABC}\, l_{BC}}{a_{ABC}}\, E_{BC} + \frac{l^D_{ABC}\, l_{CA}}{a_{ABC}}\, E_{CA} + \\ &\left. + \frac{l^C_{ABD}\, l_{BD}}{a_{ABD}}\, E_{BD} + \frac{l^C_{ABD}\, l_{DA}}{a_{ABD}}\, E_{DA} \right] = \\ &= \tfrac{\omega^2}{2} \left[\textstyle\sum_{CD} \epsilon_{ABCD} \left(d^C_{AB}\, l^D_{ABC} + d^D_{AB}\, l^C_{ABD} \right) \right] E_{AB}. \end{aligned} \tag{17}$$

Here, summation is taken over these tetrahedra $ABCD$, which possess the common edge AB. (17) has to be solved using (11) and the boundary conditions (5) and (6).

5 Eigenvalue problem

For the eigenvalue problem, we refer to the rectangular grids [2].

The transverse electric mode fields (see (5)) at the ports of a transmission line, which is discretized by means of tetrahedral grids, are computed interpolating the results of the rectangular discretization.

The field distribution at the ports is computed assuming longitudinal homogeneity for the transmission line structure. Thus, any field can be expanded into a sum of so-called modal fields which vary exponentially in the longitudinal direction:

$$\vec{E}(x,y,z \pm 2h) = \vec{E}(x,y,z)e^{\mp \jmath k_z 2h}. \tag{18}$$

k_z is the propagation constant. $2h$ is the length of an elementary cell in z-direction. We consider the field components in three consecutive elementary cells. The electric field components of the vector $\vec{e}$ (see (9)) $E_{x_{i,j,k+1}}$, $E_{x_{i,j,k-1}}$, $E_{y_{i,j,k+1}}$, $E_{y_{i,j,k-1}}$, $E_{z_{i,j,k-1}}$, $E_{z_{i+1,j,k-1}}$, and $E_{z_{i,j+1,k-1}}$ are expressed by the values of cell k using ansatz (18). The longitudinal electric field components E_z can be eliminated by means of the electric-field divergence equation (see first equation of (14)). Thus, we obtain an eigenvalue problem for the transverse electric field $\vec{y}$ on the transmission line region:

$$G\vec{y} = \gamma\vec{y}, \;\; \gamma = e^{-\jmath k_z 2h} + e^{+\jmath k_z 2h} - 2 = -4\sin^2(hk_z). \tag{19}$$

The sparse matrix G is in general nonsymmetric and complex. The order of G is $n = 2n_x n_y - n_b$. $n_x n_y$ is the number of elementary cells at the port. The size n_b depends on the number of cells with perfectly conducting material. The relation between the propagation constants k_z and the eigenvalues γ is nonlinear. The interesting modes of smallest attenuation are found solving a sequence of eigenvalue problems of modified matrices (see [4]) using the invert mode of the Arnoldi iteration [8].

6 PML modes

We use the PML in order to calculate the eigen modes of open waveguide structures as well as for structures that require electrically large computational cross sections. Using only magnetic or electric walls at the outer boundaries causes additional non-physical box modes. Those modes would affect the propagation behavior of the physical waveguide modes. Introducing the PML shifts these box modes within the eigenvalue spectrum, away from the physical ones. The difference, however, is not always large enough to be clearly detectable. Therefore, we need an additional criterion to distinguish these PML modes from the desired physical ones. The PML modes are characterized by their high power concentration in the PML area [13]. Thus, to eliminate the PML modes we calculate the magnitude of the power flow of each computed mode in the PML ($P^{(P)}$), in the waveguide region ($P^{(W)}$), and in

the total computational domain (P):

$$P = P^{(P)} + P^{(W)} = \int\limits_{\Omega^{(P)}} (\vec{E}_t \times \vec{H}^*_{t,m}) \cdot d\vec{\Omega} + \int\limits_{\Omega^{(W)}} (\vec{E}_t \times \vec{H}^*_{t,m}) \cdot d\vec{\Omega} \,. \tag{20}$$

A mode is specified as PML-mode if

$$r^{(P)} = \frac{P^{(P)}}{P} > \xi \,, \tag{21}$$

with values $\xi = 0.2, \ldots, 0.6$, found empirically.

7 Laser analysis

The presented method, although developed initially for microwave structures [3], is expanded to meet the special requirements of optoelectronic structure calculations. For optoelectronic devices frequencies of about several hundred THz are common. Thus the complex region containing the eigenvalues of potentially propagating modes grows substantially. A significantly higher number of eigenvalue problems have to be solved within our algorithm. Additionally, the maximum cell size of the discretization should be less than $\frac{\lambda}{10}$, where λ denotes the wavelength in the material with the highest $\Re([\epsilon])$. Additional mesh refinements have to be used for structure regions with highly varying fields. All this results in high-dimensional problems which have to be handled.

To reduce the execution times, in a first step the problem is solved using a coarse grid with lower accuracy requirements in order to find the approximate locations of the interesting propagation constants. Anyway, the number of modified eigenvalue problems to be solved is high. Thus, we split the interesting interval into subintervals and compute the corresponding eigenpairs independently and in parallel, for instance on different workstations or shared memory multiprocessors.

Finally, the modes of interest are calculated in a second step for an essentially reduced region using a fine grid, that fulfills higher accuracy requirements.

The linear sparse solver PARDISO [11] is applied in order to fulfill the high accuracy requirements of the eigenvalue problem. The parallel CPU mode of PARDISO provides the additional possibility to reduce the computing times for this high-dimensional problem on shared memory multiprocessors without essential additional memory requirements.

A Laser application can be found in [5].

8 Systems of linear algebraic equations

Four kinds of preconditioning and a block quasi-minimal residual algorithm are applied to solve the large scale systems of linear algebraic equations. Details are

given with [12] and [5].

Especially, adding the gradient of the electric field divergence the numerical properties of the system matrix are improved and the equations can be solved faster.

8.1 Rectangular grids

Multiplying (9) by $D_s^{1/2}$ yields a symmetric form of linear algebraic equations:

$$\bar{A}\vec{x} = 0, \quad \bar{A} = (D_s^{1/2} A^T D_{s/\tilde{\mu}} D_A^{-1} A D_s^{1/2} - k_0^2 D_{A_{\tilde{\epsilon}}}) \tag{22}$$

with $\vec{x} = D_s^{1/2}\vec{e}$. The gradient of the electric field divergence

$$[\epsilon]\nabla([\epsilon]^{-2}\nabla \cdot [\epsilon]\vec{E}) = 0 \tag{23}$$

is equivalent to the matrix equation

$$\bar{B}\vec{x} = 0, \quad \bar{B} = D_s^{-1/2} D_{A_{\tilde{\epsilon}}} B^T D_{V_{\tilde{\epsilon}\tilde{\epsilon}}}^{-1} B D_{A_{\tilde{\epsilon}}} D_s^{-1/2}. \tag{24}$$

The diagonal matrix $D_{V_{\tilde{\epsilon}\tilde{\epsilon}}}$ is a volume matrix for the 8 partial volumes of the dual elementary cell. The rectangular matrix B is sparse and contains the values 0, 1, and -1 only. Taking into account the boundary conditions (5) and (6) Eqs. (22) and (24) yields the form $\hat{A}\vec{x} = \vec{b}$ ($\hat{A} = D_s^{1/2}\tilde{A}D_s^{-1/2}$, $\vec{b} = D_s^{1/2}\vec{r}$, see (10)) and $\hat{B}\vec{x} = 0$, respectively, and

$$(\hat{A} + \hat{B})\vec{x} = \vec{b}, \;\; \hat{A} + \hat{B} \text{ complex indefinite symmetric,} \tag{25}$$

can be solved faster than (9).

In comparison to the simple lossy case the number of iterations of Krylov subspace methods increases significantly in the presence of PML. Among others the speed of convergence depends on the relations of the edges in an elementary cell of the nonequidistant rectangular grid in this case. The best results can be obtained using nearly cubic cells. Moreover, overlapping PML conditions at the corner regions of the computational domain lead to an increase of the magnitude of the corresponding off-diagonal elements in comparison to the diagonal of the coefficient matrix. This downgrades the properties of the matrix. Thus, overlapping PML should be avoided.

8.2 Tetrahedral grids

Eqs. (12) - (17) can be written in matrix form. Besides of the locations and values of the entries, these matrix representations of (12) and (13) have the same structure as (8) and (9), and an appropriate (see (22)) symmetric form of linear algebraic equations can be deduced. Adding the gradient of the electric field divergence also gives a system which can be solved faster. Here, the gradient of the divergence at an internal point is obtained considering the partial volumes of the appropriate Voronoi cell. PML are not included.

9 Application

As an example we have simulated a microwave structure with a microstrip changing its width (impedance step, see Figure 4). The discontinuity of the metallic strip

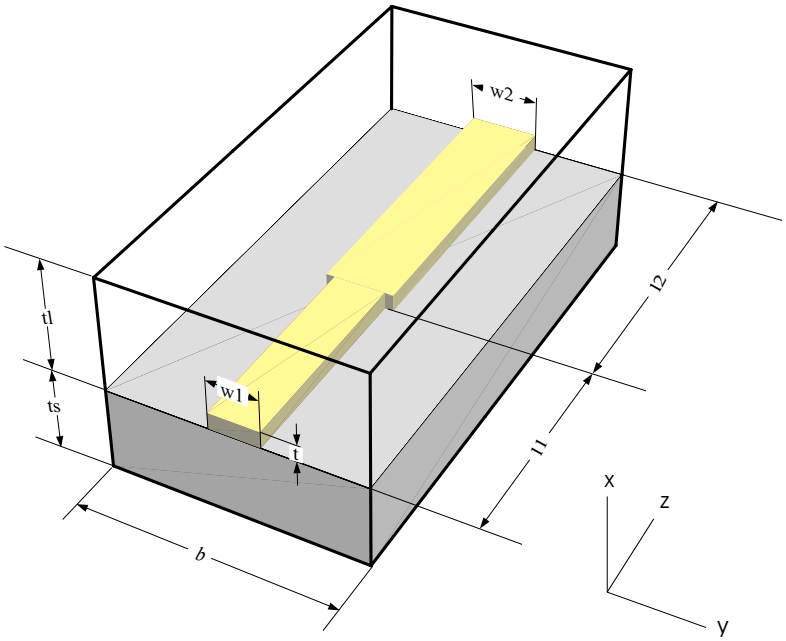

Figure 4: The microstrip line changes its extension.
Measurements: b = 300 μm, w1 = 60 μm, w2 = 80 μm, ts = 250 μm, tl = 250 μm, t = 3 μm, l1 = 200 μm, l2 = 200 μm.

is located at $z = l1$. The metal is assumed to be ideally conducting. The relative permittivity of the substrate below the microstrip line is $\epsilon_r = \tilde{\epsilon}_x = \tilde{\epsilon}_y = \tilde{\epsilon}_z = 11.9$. Above the microstrip line one has air ($\epsilon_r = \tilde{\epsilon}_x = \tilde{\epsilon}_y = \tilde{\epsilon}_z = 1$). Ports are located at the planes $z = 0$ and $z = l1 + l2$. The remaining 4 outer surfaces are assumed to be electric walls. The structure is symmetric with respect to the plane $y = b/2$. But, the whole structure is discretized in this test example.

For comparison the structure is subdivided in nonequidistant rectangular three-dimensional elementary cells on the one hand and in tetrahedra on the other hand.

In case of rectangular grids, the order of the system of linear algebraic equations, which corresponds to the boundary value problem (1), is $n = 3n_x n_y n_z = 335\,160$. $n_x n_y n_z$ is the number of cells of the structure which is assumed to be a parallelepiped. We need a high mesh refinement near the microstrip line. Using the rectangular grid the mesh refinement in this region results in an accumulation of elementary cells in all coordinate directions even though the refinement is not necessary in order to approximate the solution with the required accuracy.

The tetrahedral grid consists of $n_n = 29\,615$ nodes, $n_t = 161\,308$ tetrahedra, and $n_p = 16\,100$ peripheral cell faces. The order of the corresponding system of linear algebraic equations is equal to the number of edges and amounts

$$n = n_n + n_t + n_p/2 - 1 = 198\,972. \tag{26}$$

The disadvantage of rectangular grids, the accumulation of elementary cells in all coordinate directions, is avoided here.

10 Conclusions

Finite-difference analysis of microwave circuits including lossy materials and radiation effects leads to an complex eigenvalue problem and large-scale complex indefinite symmetric systems of linear algebraic equations. Staggered nonequidistant rectangular grids and tetrahedral nets with corresponding Voronoi cells are used. The high execution times in the eigenvalue problems for waveguide applications with extremely large mesh sizes, e.g. laser structures, are reduced using a coarse and a fine grid, and two levels of parallelization. The high-dimensional systems of linear algebraic equations are solved using a bock Krylov subspace method.

Acknowledgements. We thank F.-K. Hübner for his support in preparing graphics.

References

[1] Klaus Beilenhoff, Wolfgang Heinrich, and Hans L. Hartnagel. Improved finite-difference formulation in frequency domain for three-dimensional scattering problems. *IEEE Transactions on Microwave Theory and Techniques*, 40, No. 3:540–546, 1992.

[2] Andreas Christ and Hans L. Hartnagel. Three-dimensional finite-difference method for the analysis of microwave-device embedding. *IEEE Transactions on Microwave Theory and Techniques*, 35:688–696, 1987.

[3] Georg Hebermehl, Friedrich-Karl Hübner, Rainer Schlundt, Thorsten Tischler, Horst Zscheile, and Wolfgang Heinrich. Numerical simulation of lossy microwave transmission lines including PML. *Lecture Notes in Computational Science and Engineering, Springer Verlag*, 18:267–275, 2001.

[4] Georg Hebermehl, Friedrich-Karl Hübner, Rainer Schlundt, Thorsten Tischler, Horst Zscheile, and Wolfgang Heinrich. Perfectly matched layers in transmission lines. *Numerical Mathematics and Advanced Applications, ENUMATH 2001, Springer Verlag Italia*, pages 281–290, 2003.

[5] Georg Hebermehl, Friedrich-Karl Hübner, Rainer Schlundt, Thorsten Tischler, Horst Zscheile, and Wolfgang Heinrich. Simulation of microwave and semiconductor laser structures including absorbing boundary conditions. *Lecture Notes in Computational Science and Engineering, Springer Verlag*, 35:131–159, 2003.

[6] Georg Hebermehl, Rainer Schlundt, Horst Zscheile, and Wolfgang Heinrich. Simulation of monolithic microwave integrated circuits. WIAS Preprint no. 235, Weierstraß-Institut für Angewandte Analysis und Stochastik, 1996.

[7] Georg Hebermehl, Rainer Schlundt, Horst Zscheile, and Wolfgang Heinrich. Improved numerical methods for the simulation of microwave circuits. *Surveys on Mathematics for Industry*, 9:117–129, 1999.

[8] R. B. Lehoucq. Analysis and implementation of an implicitly restarted Arnoldi iteration. Technical Report **13**, Rice University, Department of Computational and Applied Mathematics, 1995.

[9] Z. S. Sacks, D. M. Kingsland, R. Lee, and J.-F. Lee. A perfectly matched anisotropic absorber for use as an absorbing boundary condition. *IEEE Transactions on Antennas and Propagation*, 43:1460–1463, 1995.

[10] Jürgen Schefter. Discretisation of the Maxwell equations on tetrahedral grids. WIAS Technical Report no. 6, Weierstraß-Institut für Angewandte Analysis und Stochastik, 2003.

[11] O. Schenk, K. Gärtner, and W. Fichtner. Efficient sparse LU factorization with left-right looking strategy on shared memory multiprocessors. *BIT*, 40:158–176, 2000.

[12] Rainer Schlundt, Georg Hebermehl, Friedrich-Karl Hübner, Wolfgang Heinrich, and Horst Zscheile. Iterative solution of systems of linear equations in microwave circuits using a block quasi-minimal residual algorithm. *Lecture Notes in Computational Science and Engineering, Springer Verlag*, 18:325–333, 2001.

[13] Thorsten Tischler and Wolfgang Heinrich. The perfectly matched layer as lateral boundary in finite-difference transmission-line analysis. *IEEE Transactions on Microwave Theory and Techniques*, 48:2249– 2253, 2000.

[14] T. Weiland. A discretization method for the solution of Maxwell's equations for six-component fields. *Electronics and Communication (AEÜ)*, 31:116–120, 1977.